

Fluctuating Cu-O-Cu Bond model of high temperature superconductivity in cuprates

D. M. Newns and C. C. Tsuei

IBM T.J. Watson Research Center, Yorktown Heights, NY 10598

(June 8 2006)

Abstract

Twenty years of extensive research has yet to produce a general consensus on the origin of high temperature superconductivity (HTS). However, several generic characteristics of the cuprate superconductors have emerged as the essential ingredients of and/or constraints on any viable microscopic model of HTS. Besides a T_c of order 100 K, the most prominent on the list include a d-wave superconducting gap with Fermi liquid nodal excitations, a d-wave pseudogap with the characteristic temperature scale T^* , an anomalous doping-dependent oxygen isotope shift, nanometer-scale gap inhomogeneity, etc.. The key role of planar oxygen vibrations implied by the isotope shift and other evidence, in the context of CuO_2 plane symmetry and charge constraints from the strong intra- $3d$ Coulomb repulsion U , enforces an anharmonic mechanism in which the oxygen vibrational amplitude modulates the strength of the in-plane Cu-Cu bond. We show, within a Fermi liquid framework, that this mechanism can lead to strong d-wave pairing and to a natural explanation of the salient features of HTS.

Great strides towards understanding HTS have been made during the last twenty years of intense experimental and theoretical research on cuprate superconductors [1], [2]. However, there is no general consensus on the origin of HTS. Especially there is no report on a specific microscopic pairing mechanism that is capable of encompassing the complex phenomenology of the superconducting and normal states consistently in one theoretical model.

Among the highly unconventional properties of the cuprate superconductors are the d -wave symmetry of the superconducting gap [3] and the presence of a pseudogap *also* with d -wave symmetry [4]. Theoretical insight is provided by study of the low-energy excitations around the node in the d -wave gap, where disparate low-temperature experiments including specific heat [5], transport [6], [7], [8], [9], [10], [11], and penetration depth [12], together with angle-resolved photoemission spectroscopy (ARPES) [13] can all be interpreted in terms of a Fermi liquid description. This suggests the plausibility of a broadly BCS framework [2], of which an important consequence is that the large on-site Coulomb repulsion U [14] does not enter into d -wave pairing to first order.

In conventional superconductivity the isotope exponent α has been key in signalling the role of phonons in the pairing mechanism. HTS exhibits a universal, anomalous doping-dependent isotope shift [15], [16] which shows that phonons are again playing a key role, but in some unconventional manner, and any viable microscopic model must be able to account for this. A further challenge to theory is the recently observed spatial inhomogeneity of the gap at the nanometer scale [17].

Recently interest in the role of electron-phonon coupling has been rekindled by mounting experimental support, which, in addition to the isotope shift, includes electronic Raman scattering, [18], [19], ARPES [20], [21], [22], [23], inelastic neutron scattering [24], x-ray absorption fine structure [25], low-temperature STM/STS [26], and isotope effect in penetration depth measurements [27]. Extensive theoretical studies [28], [29], [30] [31], [32], [33], [34], [20], [35], [36] have shed light on the relevance of electron-phonon interaction in understanding HTS.

Here, in re-examining phonon coupling, we find a novel microscopic pairing mechanism which can indeed explain the essence of HTS phenomena: high T_c 's, d -wave pairing, d -symmetry pseudogap, anomalous isotope shift, and nanoscale gap inhomogeneity. Although the effects of U are manifested [14], here we shall focus on interactions directly responsible for pairing, allowing for U *indirectly* by decoupling from on-site charge fluctuations. We

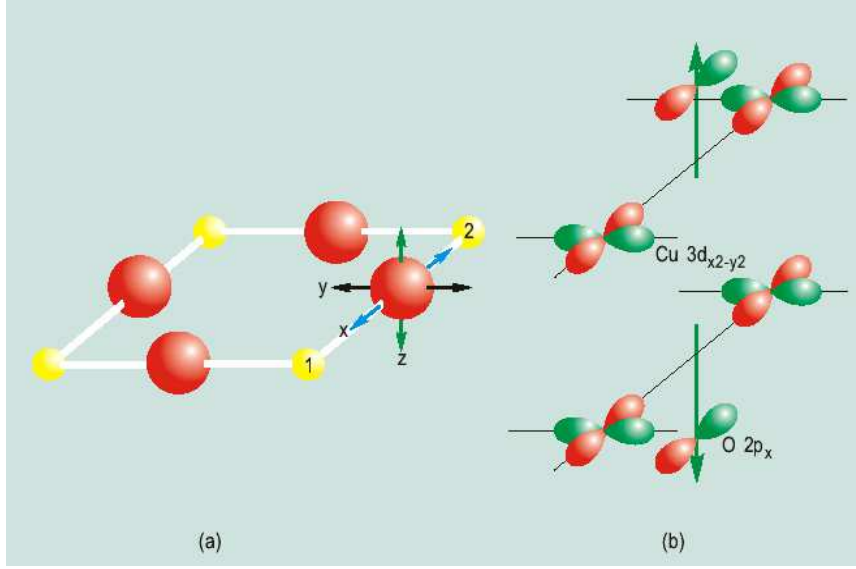


FIG. 1: (a) The unit cell in the CuO₂ plane, with Cu atoms (yellow) and O atoms (red), showing x , y , and z vibrational modes (arrows). (b) The Cu $3d_{x^2-y^2}$ and O $2p_x$ orbitals, illustrating effect of an O z -displacement (green arrows), positive sense (top panel), and negative sense (bottom panel).

start by considering how oxygen vibrations can modify electronic motion in the CuO₂ plane, the universal active component of HTS materials. The CuO₂ plane is a square lattice of divalent Cu ions with oxygen ions located at the centers of the Cu-Cu bond (Fig. 1a). Only the highest-lying $3d_{x^2-y^2}$ orbital (Fig. 1b) plays an active role, crystal field effects demoting the other Cu $3d^9$ orbitals to core-like status.

Let us look at a single Cu-Cu bond between $3d_{x^2-y^2}$ orbitals located on atoms labeled 1 and 2 (Fig. 1). The kinetic energy associated with the unperturbed direct bond 1-2 comes, within a one-band model, from the nearest-neighbor hopping matrix element t

$$h_{12}^e = -t \sum_{\sigma} (c_{1,\sigma}^+ c_{2,\sigma} + c_{2,\sigma}^+ c_{1,\sigma}), \quad (1)$$

where the $c_{i,\sigma}^+$ ($c_{i,\sigma}$) are Fermion creation (destruction) operators for Cu site i and spin σ . The intersite hopping actually occurs via superexchange, i.e. wavefunction overlap between the $3d_{x^2-y^2}$ orbital of Cu1, the intrabond oxygen $2p_x$ longitudinal with the bond, and the $3d_{x^2-y^2}$ orbital of Cu2 (Fig. 1b), sensitizing it to the local oxygen vibrational degrees of

freedom (Fig. 1a). Consider the effect, sketched in Fig. 1b, of, for example, the out-of-plane oxygen displacement z , which is to reduce the overlap between both $3d_{x^2-y^2}$ orbitals and the oxygen $2p_x$ orbital, thus reducing the effective coupling t . But due to the local centrosymmetry of the O-site, this t -reduction effect is the same irrespective of the sign of the displacement z , so that its lowest order expression is as z^2 . Hence the electron-vibrator term in the Hamiltonian must have the unusual second order form of coupling

$$h_{12}^{ev} = \frac{v}{2} z^2 \sum_{\sigma} (c_{1,\sigma}^+ c_{2,\sigma} + c_{2,\sigma}^+ c_{1,\sigma}), \quad (2)$$

where v is the coupling strength. This electron-vibrator coupling causes the Cu-Cu bond strength t to *fluctuate* with the oxygen vibrator square amplitude z^2 - hence the description Fluctuating Bond Model (FBM). The two other oxygen vibrational modes, x and y , can also couple to the bond strength in a similar manner. In addition to coupling to the bond, the vibrational mode x , longitudinal to the bond, can also displace charge onto the Cu1 and Cu2 sites; however since charge accumulation on the Cu sites is resisted by the large intrasite Coulomb interaction U , we do not believe that on-site charge displacement can be important, and ignore it in our model at the present maximally simplified stage.

The oxygen vibrational degree of freedom needs to embody an anharmonic potential term in a theory with nonlinear electron-vibrator coupling, e.g. for the z -mode the vibrator Hamiltonian should have the form

$$h_{12}^v = \frac{p_z^2}{2m} + \frac{1}{2} m \omega_0^2 z^2 + \frac{w}{8} z^4, \quad (3)$$

where a fourth-order potential with coefficient w (again, centrosymmetry is used to eliminate a cubic term) has been included, in addition to the conventional harmonic terms in which p_z is oxygen momentum, m effective mass, and ω_0 the harmonic vibrator frequency. The potential may be a flattened well or a double well, depending on the sign of ω_0^2 (see Fig. 2a). A quartic anharmonic potential is not unique in perovskite physics, a similar potential plays a key role in the theory of ferroelectricity [37].

In the following the FBM Pairing Interaction will be derived systematically. First, we give a non-rigorous argument leading to a physical picture of the pairing by completing the square in the highest-order interaction. Introducing the compact notation X_{12} as the bond order operator, describing the strength of the Cu1-Cu2 electronic coupling,

$$X_{12} = \sum_{\sigma} (c_{1,\sigma}^+ c_{2,\sigma} + c_{2,\sigma}^+ c_{1,\sigma}), \quad (4)$$

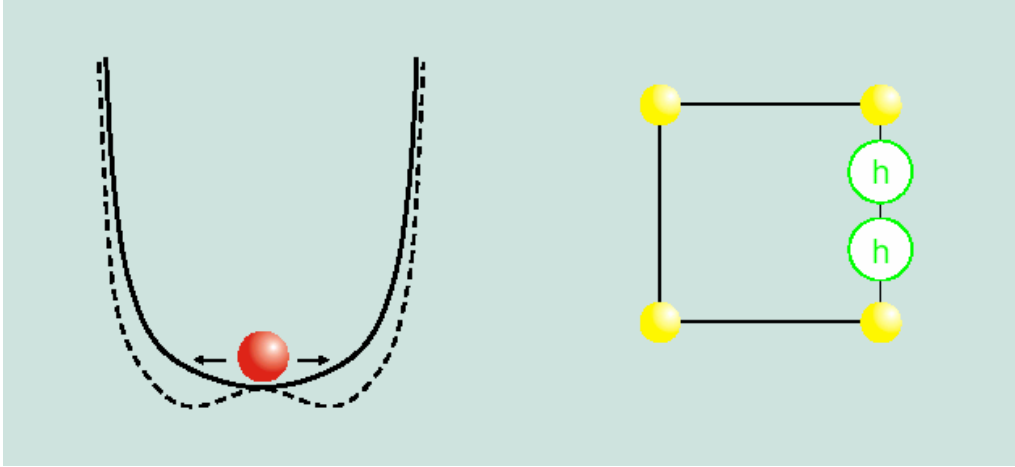


FIG. 2: Left (a): Bare oxygen anharmonic potential (3) full (dashed) curves with positive (negative) harmonic coefficient $m\omega_0^2$. Right (b): Binding of two quasiparticles (e.g. holes h) in a Cu-Cu bond, as given by Eq. (5).

and completing the square (classically valid in the Fig 2a double well case when $-m\omega_0^2 \gg v \langle X_{12} \rangle$)

$$\frac{w}{8}z^4 + \frac{vz^2}{2}X_{12} = \frac{w}{8} \left(z^2 + \frac{2v}{w}X_{12} \right)^2 - \frac{K}{2}X_{12}^2, \quad (5)$$

we find a new, **attractive** electron-electron (or hole-hole) interaction in the intra-bond channel, of strength K , where $K = v^2/w$. K is the key interaction in the FBM. Because the interaction K acts via the bond operator X_{12} , it is seen from the form X_{12}^2 to lie in the intra-bond channel (see Fig. 2b) as opposed to being on-site, and with the y -bond included the Fourier transform of the interaction leads to the d-wave factor $\cos q_x - \cos q_y$, resulting in pairing and pseudogap phenomena of *d-wave symmetry*. There is experimental evidence for linking the HTS pairing mechanism with the oxygen z -vibrational mode: if the vibrator is localized in the z -direction by large static CuO_2 plane buckling [38], T_c is reduced and can go to zero. Hence a key role in pairing must indeed be played by the oxygen degree of freedom.

We are now ready to write down the complete FBM Hamiltonian, as a sum of electronic,

vibrator, and coupling terms:

$$H^{FBM} = H^e + H^v + H^{ev}. \quad (6)$$

Here the electronic term includes hopping over longer ranges than the nearest neighbor hopping considered in Eq(1):

$$H^e = -\frac{1}{2} \sum_{\mathbf{i}, \mathbf{j}, \sigma} t(\mathbf{i} - \mathbf{j}) c_{\mathbf{i}, \sigma}^+ c_{\mathbf{j}, \sigma}, \quad (7)$$

where \mathbf{i} denotes the $3d_{x^2-y^2}$ orbital on lattice site $\mathbf{i} = (i_x, i_y)$ in the 2D square lattice of Cu ions. The strongest interaction is the nearest neighbor hopping integral $t(\pm 1, 0) = t(0, \pm 1) = t$, followed by the next-nearest neighbor interaction $t(\pm 1, \pm 1) = t'$, and then the 3rd-nearest neighbor interaction $t(\pm 2, 0) = t(0, \pm 2) = t''$. The band eigenvalues $\epsilon_{\mathbf{k}}$ of (7) are $\epsilon_{\mathbf{k}} = -2t(\cos k_x + \cos k_y) - 4t' \cos k_x \cos k_y - 2t''(\cos 2k_x + \cos 2k_y)$ in units where lattice constant= 1.

In the vibrational term

$$H^v = \sum_{\mathbf{i}, \alpha} \left[\frac{1}{2m} p_{\mathbf{i}, \alpha}^2 + \frac{m\omega_0^2}{2} x_{\mathbf{i}, \alpha}^2 + \frac{w}{8n} (x_{\mathbf{i}, \alpha}^2)^2 \right], \quad (8)$$

the bonds are relabelled for greater notational convenience, in terms of a Cu site \mathbf{i} and a direction $\alpha = x$ or y away from \mathbf{i} in the positive axis direction. The vibrational modes are approximated as local (Einstein) and isotropic. The notation p^2, x^2 implies $\sum_s p_s^2, \sum_s x_s^2$ where s is polarization ($s =$ transverse to plane, longitudinal to bond, or in plane transverse to bond). The mode degeneracy is n .

The bond order operators are defined using the same bond notation

$$X_{\mathbf{i}, \alpha} = \sum_{\sigma} \left[c_{\mathbf{i}, \sigma}^+ c_{\mathbf{i} + \hat{\mathbf{x}}_{\alpha}, \sigma} + c_{\mathbf{i} + \hat{\mathbf{x}}_{\alpha}, \sigma}^+ c_{\mathbf{i}, \sigma} \right], \quad (9)$$

where $\hat{\mathbf{x}}_{\alpha}$ is a unit vector along the direction α . In terms of these, the coupling Hamiltonian is

$$H^{ev} = \frac{v}{2\sqrt{nn_s}} \sum_{\mathbf{i}, \alpha} x_{\mathbf{i}, \alpha}^2 X_{\mathbf{i}, \alpha}. \quad (10)$$

The prefactor includes a spin degeneracy n_s .

To solve the FBM we shall in this paper use the standard weak-coupling approach, based on an electron gas as the unperturbed system. To develop a perturbation expansion in the absence of the Migdal theorem in HTS [3], we adopt the $1/N$ expansion technique, where

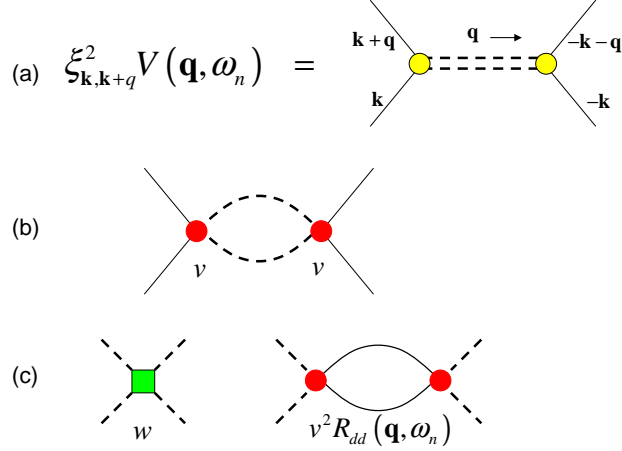


FIG. 3: (a) The interaction between two pairing quasiparticles \mathbf{k} and $-\mathbf{k}$, exchanging momentum \mathbf{q} and frequency ω_n , is a product of d -wave form factors $\xi_{\mathbf{k},\mathbf{k}+\mathbf{q}}^2$ (yellow circles) and potential propagator $V(\mathbf{q}, \omega_n)$. (b) First approximation to V based on $v^2 \times$ two-boson propagator. Dashed lines represent single vibrator (boson) propagator, red circles electron-boson interaction v . (c) The leading- N self-energy corrections to V (see analogous corrections in the heavy fermion problem [41]) come from boson-boson interaction w and $v^2 \times$ Response Function R_{dd} . Full lines represent fermion quasiparticle propagator. Green square represents boson-boson interaction w , fermion lens is response Function R_{dd} .

N is degeneracy, e.g. orbital or spin degeneracy. The $1/N$ expansion works well e.g. for the Kondo problem [39], the results remaining physical down to spin degeneracy $N = 2$. Here we systematically co-expand in the inverse of the mode degeneracy n and the spin degeneracy n_s using a path integral approach [40] (see supplementary material), meaning by expressions such as " $1/N$ " the joint orders $1/n$ and $1/n_s$.

The interaction which scatters a pair $(\mathbf{k}, -\mathbf{k})$ to $(\mathbf{k} + \mathbf{q}, -\mathbf{k} - \mathbf{q})$ (Fig. 3) differs from the usual single phonon propagator structure in BCS, because there is no single electron-phonon interaction term in the FBM Eq's (6-10). The structure is instead a *two-boson* propagator (Fig. 3b) with self-energy insertions, the leading- N self energy involving the boson-boson interaction w and $v^2 \times$ a fermion response function (Fig. 3c). Because the response function can go from bond $\alpha = x$ or y to bond $\beta = x$ or y it is a 2×2 matrix.

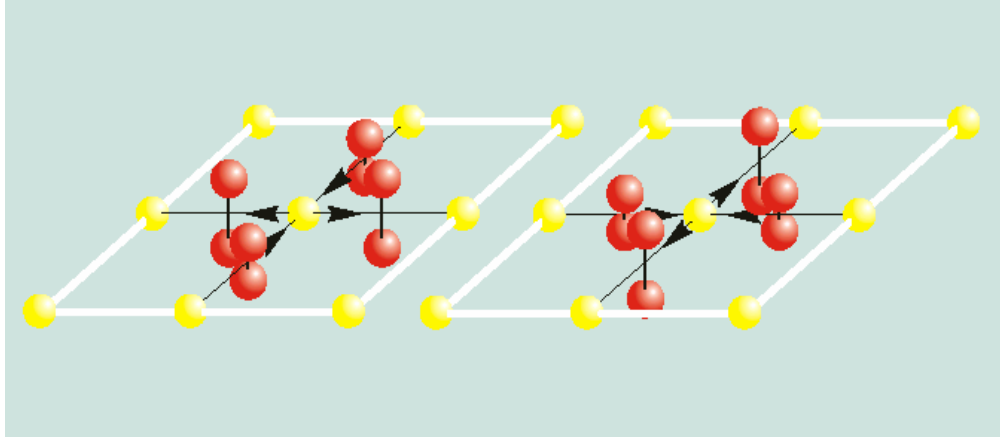


FIG. 4: The Fluctuating Bond field after projecting out s -fluctuations has d -symmetry, with (left panel) O-amplitude (dumbbells) large in y -bonds, small in x -bonds, the reverse in right panel. Panels also illustrate opposite phases of the static d -wave CDW (18).

The matrix can be simplified by noticing the dramatic *divergence* produced by the self-energy insertions at small transferred wavevector q . This small- q divergence comes from fluctuations having d -wave symmetry, the s -wave part being nonsingular and uninteresting. Therefore, our simplifying procedure is to reduce the 2×2 propagator matrix to a scalar by projecting out s -symmetry charge fluctuations and retaining only the d -symmetry ones, the projection procedure being implemented in path integral formalism (see supplementary material). The vibrator amplitude/ X -operator fluctuations around each Cu site now form a $d_{x^2-y^2}$ -like pattern (see Fig. 4). This selection of the d -channel has the additional physical merit that charge flow into and out of each Cu site is balanced (Fig. 4), i.e. there is zero net site charge accumulation, compatible with the accepted large Coulomb repulsion U on each site, which inhibits such charge fluctuations.

The FBM pairing propagator $\Gamma(\mathbf{k}, \mathbf{q}, n)$ (Fig. 3) for scattering a pair from $(\mathbf{k}, -\mathbf{k})$ to $(\mathbf{k} + \mathbf{q}, -\mathbf{k} - \mathbf{q})$ is now given (for a full derivation see supplementary material) by the Fig. 3 graphs as a product of d -wave form factors and a 2-phonon potential propagator $\mathbf{V}(\mathbf{q}, n)$

$$\Gamma(\mathbf{k}, \mathbf{q}, n) = |\xi_{\mathbf{k}, \mathbf{k}+\mathbf{q}}|^2 \mathbf{V}(\mathbf{q}, n), \quad (11)$$

where the d -type form factor (coming from the form factor of the bond operator X) is

$$\xi_{\mathbf{k},\mathbf{k}'} = \frac{1}{2} [\cos(k_x) + \cos(k'_x) - \cos(k_y) - \cos(k'_y)], \quad (12)$$

and the potential propagator (dropping a zero-frequency term, only significant at temperatures above those of interest) is

$$\mathbf{V}(\mathbf{q}, n) = \frac{-4n_s^{-1}K\omega_a^2 f_{\mathbf{q}}}{\omega_n^2 + 4\bar{\omega}^2 + 4\omega_a^2 f_{\mathbf{q}} \left[\frac{1}{2} - KR_{dd}(\mathbf{q}, n) \right]}. \quad (13)$$

Here $\omega_n = 2\pi n k_B T$ is the Matsubara frequency (Fourier component with respect to imaginary time), T =temperature, k_B =Boltzmann's constant, and we introduce definitions of the total vibrator frequency $\bar{\omega}$, the mean field harmonic vibrator frequency ω_h , and the anharmonic component of the vibrator frequency ω_a

$$\begin{aligned} \bar{\omega}^2 &= \omega_h^2 + \omega_a^2, \\ \omega_h^2 &= \omega_0^2 + \frac{v}{m} \langle X_{\mathbf{i},\alpha} \rangle, \\ \omega_a^2 &= \frac{w}{2m} \langle x_{\mathbf{i},\alpha}^2 \rangle = \frac{w}{4m^2\bar{\omega}} \coth\left(\frac{\bar{\omega}}{2k_B T}\right). \end{aligned} \quad (14)$$

In the denominator of (13) we can identify (in square brackets) the two terms in the self energy (Fig. 3c), the positive one coming from w , and the negative one coming from $v^2 R_{dd}$. The other two terms are the inverse of the two-boson propagator (Fig. 3b) with characteristic frequency $2\bar{\omega}$ (a frequency up-shifted by the single-boson self energy). The form factor $f_{\mathbf{q}}$ is defined by $f_{\mathbf{q}} = \frac{1}{2} [\cos^2(q_x/2) + \cos^2(q_y/2)]$, and the dd Response Function R_{dd} is defined in the normal state as

$$R_{dd}(\mathbf{q}, n) = - \sum_{\mathbf{k}} \frac{f(\epsilon_{\mathbf{k}}) - f(\epsilon_{\mathbf{k}+\mathbf{q}})}{i\omega_n + \epsilon_{\mathbf{k}} - \epsilon_{\mathbf{k}+\mathbf{q}}} \xi_{\mathbf{k},\mathbf{k}+\mathbf{q}} \xi_{\mathbf{k}+\mathbf{q},\mathbf{k}}, \quad (15)$$

where $f(\epsilon_{\mathbf{k}})$ is the Fermi function. The dd Response Function (RF) is a generalization of the density-density RF. The presence of the ξ -factors shows that the RF can be interpreted as the d -symmetry density response to a d -symmetry perturbation. At long wavelengths, the RF is decoupled from the on-site fluctuations of s -symmetry, hence it is decoupled from the strong on-site Coulomb repulsion U .

The modified 2-phonon interaction $\mathbf{V}(\mathbf{q}, n)$ can diverge at low frequency and small q , at significant values of the interaction K , due to the largeness of R_{dd} when the Fermi level lies at the energy ϵ_{SP} of the saddle points (SP) (or "antinodal points") at $\mathbf{k} = (\pi, 0)$ and $(0, \pi)$

in the band structure, signaling the emergence of a 2-phonon bound state. The same SP effect causes a peak, the van Hove singularity, in the density of states (DOS) at energy ϵ_{SP} . In this situation the superconducting gap acts, through controlling the magnitude of R_{dd} , to regularize the divergence.

Let us now look at the leading- N gap equation at T_c

$$\Delta(\mathbf{k}, n) = -T \sum_{\mathbf{k}', n'} \xi_{\mathbf{k}, \mathbf{k}'}^2 \mathbf{V}(\mathbf{k} - \mathbf{k}', n - n') G_2(\mathbf{k}', n') \Delta(\mathbf{k}', n'), \quad (16)$$

where $\Delta(\mathbf{k}, n)$ is the gap and $G_2(\mathbf{k}, n) = (\nu_n^2 + \epsilon_{\mathbf{k}}^2)^{-1}$.

In standard BCS theory, G_2 gives rise to a log divergence in T , which results in a solution to the gap equation with the well-known standard BCS formula for T_c exponential in the inverse coupling constant. In contrast, in the FBM there is the stronger divergence in $\mathbf{V}(\mathbf{q}, m)$, which tends to peg T_c at the temperature where the divergence disappears. Since this temperature is defined by the denominator in $\mathbf{V}(\mathbf{q}, m)$, in which no degeneracy factor n_s appears, it is a leading- N formula. Hence we are justified in neglecting the second Eliashberg equation involving electronic mass renormalization (Z -factor) as a $1/N$ correction.

Solving the gap equation, we always find a $d_{x^2-y^2}$ -wave gap $\Delta(\mathbf{k}, n)$ due to the $\xi_{\mathbf{k}, \mathbf{k}'}^2$ factors - originating in the FBM pairing interaction being localized on a bond (Fig. 2b) - and to the largeness of the $V(\mathbf{q}, n)$ at small q . In Fig. 5a we present some results for T_c and oxygen isotope shift (the technique used was to solve at finite gap using Fast Fourier Transform (FFT) techniques [42], and extrapolate to zero gap) as a function of doping. The results show the standard hump in T_c as function of doping, and a very dramatic minimum in the isotope shift going down to almost zero around the T_c -maximum, while going up to values above the BCS $\alpha = 0.5$ on the underdoped side. In Fig. 5b we present experimental results for the "universal" isotope shift behavior found for several materials [15], [16] along with the widely used "universal" empirical formula for T_c [43]. It is seen that there is a remarkable semiquantitative agreement between theory and experiment, which is especially remarkable as the isotope shift in BCS theory is quite robust.

The explanation for the hump in T_c as a function of doping in the FBM, is that the density of states and the RF peak around the point where the Fermi energy coincides with the band structure energy ϵ_{SP} at the SP. At this point a zero in the denominator of the pairing interaction $\mathbf{V}(\mathbf{q}, m)$ is more readily obtained, while high DOS always favors pairing. The phonon parameters in Fig. 5 have been selected so that the phonon frequency is

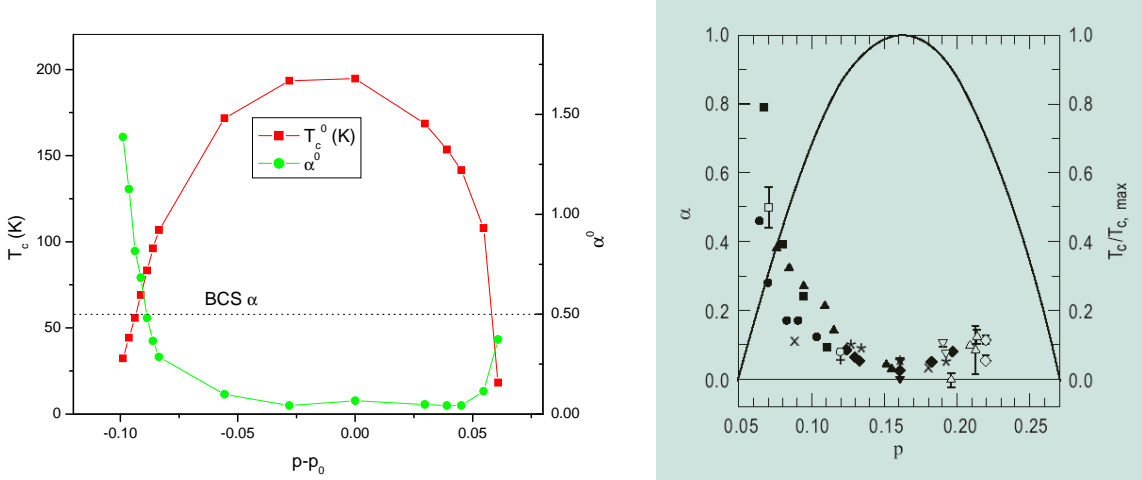


FIG. 5: (a) Left panel. Transition temperature T_c and oxygen isotope shift α^0 vs. doping p , relative to doping p_0 at max. T_c , from gap equation (16). Parameters $t = 0.25$ eV, $t' = -0.06$ eV, $t'' = 0.0325$ eV, $K = 0.48$ eV, $\omega_a = 0.05$ eV, $\omega_h = 0.015$ eV. Phonon frequencies in this range are reported by ref's [18]-[25](b) Right panel. Experimental transition temperature and isotope shift. Full curve, empirical T_c -doping relation $T_c = T_{c, \max}(1 - 82.6(p - p_0)^2)$ [43]. Points are oxygen isotope shift measurements for YBCO-based and Bi-2212 cuprate superconductors [16].

mainly of anharmonic origin, i.e. a mainly quartic potential (see Fig. 2a), when the zero in the denominator of $\mathbf{V}(\mathbf{q}, n)$ is mass-independent (ω_a factors out), hence the extremely low isotope shift. As the Fermi energy moves away from ϵ_{SP} , the DOS drops and the FBM divergence in the pairing interaction tends to disappear, with a resumption of more normal BCS isotope shift.

As well as driving pairing, the coupling K can also produce static distortions. The 2-phonon interaction w can be renormalized to \tilde{w} by summing a somewhat more extended set of leading- N Feynman diagrams than those in Fig. 2. \tilde{w} is found to contain the proportionality factor

$$\tilde{w} \sim \frac{1}{2} - KR_{dd}(\mathbf{q}, n), \quad (17)$$

leading to a zero in the long-wavelength \tilde{w} at a temperature T_{mf} . Below T_{mf} there is symmetry-breaking in the system, which can be likened to the presence of an Ising pseudospin

in each unit cell. The symmetry breaking can be described in real space as a local splitting of the nearest-neighbor hopping integrals t , $t_x \neq t_y$, and in \mathbf{k} -space as a splitting of the saddle point energies at the k -points X and Y, $\epsilon_{SP}^X \neq \epsilon_{SP}^Y$.

An ordered pseudospin structure has been sought in the form of a 1D d -wave CDW [44], with the Ansatz

$$u_{\mathbf{i}}^2 = \frac{2\sqrt{nn_s}}{v} \chi_{\mathbf{Q}} \cos(\mathbf{Q} \cdot \mathbf{i}), \quad (18)$$

where

$$u_{\mathbf{i}}^2 = \frac{1}{2} (x_{\mathbf{i}+\hat{x}/2}^2 + x_{\mathbf{i}-\hat{x}/2}^2 - y_{\mathbf{i}+\hat{y}/2}^2 - y_{\mathbf{i}-\hat{y}/2}^2), \quad (19)$$

and $\mathbf{Q} = (Q_x, Q_y)$ is the CDW wavevector. The d -wave nature of the CDW is seen in that the expression (19) corresponds to a static distortion of the type represented in Fig. 4.

The propagator $G(\mathbf{k}, n)$, in a standard approximation where the self-energy is second order in $\chi_{\mathbf{Q}}$, is given by

$$G(\mathbf{k}, n) = \frac{1}{i\nu_n - \epsilon_{\mathbf{k}} - \chi_{\mathbf{Q}}^2 \Phi(\mathbf{k}, n)}, \quad (20)$$

with

$$\Phi(\mathbf{k}, n) = \frac{1}{4} \left[\frac{\xi_{\mathbf{k}, \mathbf{k}+\mathbf{Q}}^2}{i\nu_n - \epsilon_{\mathbf{k}+\mathbf{Q}}} + \frac{\xi_{\mathbf{k}, \mathbf{k}-\mathbf{Q}}^2}{i\nu_n - \epsilon_{\mathbf{k}-\mathbf{Q}}} \right]. \quad (21)$$

By calculating the free energy, the wavevector \mathbf{Q} was determined by energy minimization. The direction of \mathbf{Q} is found to lie along the x - or y - axis, $\mathbf{Q} = (Q, 0)$, or $= (0, Q)$. The CDW is found to be stable - relative to the uniformly-polarized (but presumably disordered) state - below a temperature T_{CDW} , which is plotted in Fig. 6, a stability mostly confined to the underdoped side. Q in this region closely tracks the nesting wavevector between the two pieces of Fermi surface at X or Y in the band structure (inset Fig. 6). Note the discrepancy in the empirical K -value between Figures 5 and 6. A large hidden negative contribution to the empirical K can be assumed from the nearest-neighbor Coulomb repulsion V . In a superconducting context, Coulomb interactions are reduced to a lower value V^* by off-shell scattering, while there is no such effect for the static CDW. Hence the CDW effective K should be less attractive, with the two K -values differing by roughly $V - V^*$.

The CDW-induced modification to the energy band structure can be seen by looking at the poles in the propagator $G(\mathbf{k}, n)$ lying at low energy. Suppose that $\epsilon_{\mathbf{k}}$ and $\epsilon_{\mathbf{k}+\mathbf{Q}}$ lie near the Fermi level (\mathbf{k} and $\mathbf{k} + \mathbf{Q}$ are 2 points related by nesting), when $\epsilon_{\mathbf{k}-\mathbf{Q}}$ will typically lie far away so only the term in $\epsilon_{\mathbf{k}+\mathbf{Q}}$ in Φ diverges. Then the poles are approximately at

$$i\nu_n = \epsilon_F \pm \frac{1}{2} \chi_{\mathbf{Q}} \xi_{\mathbf{k}, \mathbf{k}+\mathbf{Q}} \rightarrow \epsilon_F \pm \chi_{\mathbf{Q}}, \quad (22)$$

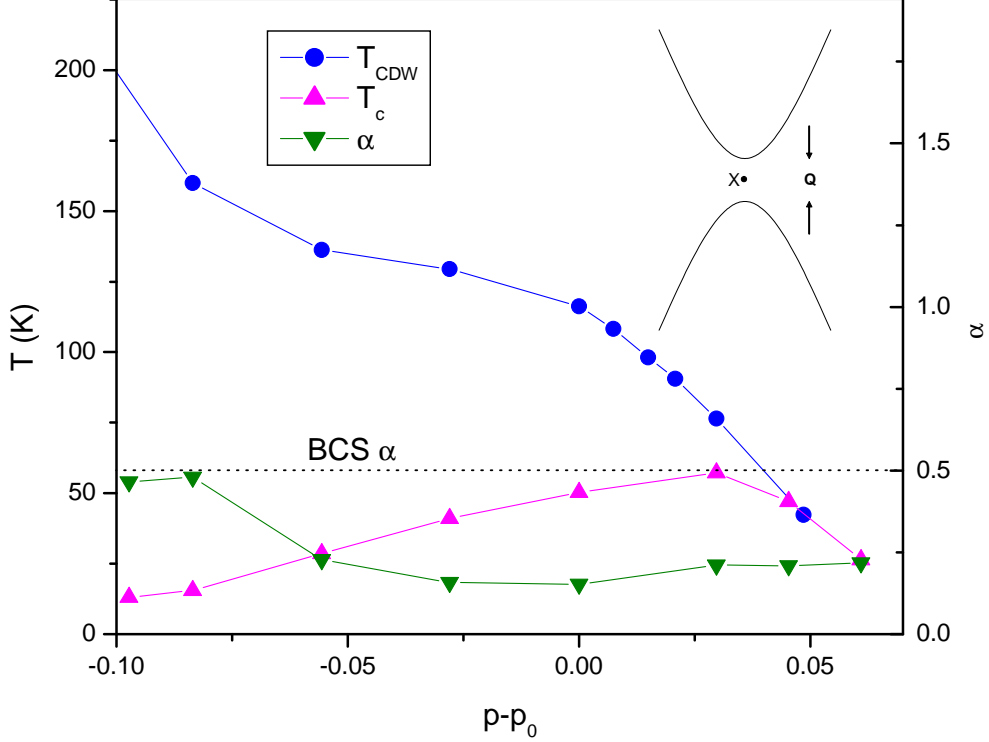


FIG. 6: T_{CDW} (blue circles) calculated from stability boundary of CDW relative to uniform solution. T_c (magenta triangles) and α (green triangles) calculated in presence of CDW from LG equation. Inset shows nesting wavevector \mathbf{Q} at point $X = (\pi, 0)$ in BZ. Parameters as Fig. 5, except $K = 0.23$ eV in T_{CDW} calculation (see text).

where $\xi_{\mathbf{k}, \mathbf{k}+\mathbf{Q}} \simeq \pm 2$. An identical argument can be made for the case of scattering from \mathbf{k} to $\mathbf{k} - \mathbf{Q}$. Hence we see that $\chi_{\mathbf{Q}}$ is the gap opened up by the breakdown in long range order caused by the CDW - it is a form of pseudogap. The factor $\xi_{\mathbf{k}, \mathbf{k}+\mathbf{Q}}$, which is approximately $\cos k_x - \cos k_y$ at the small Q of interest, shows the presence of a d -wave symmetry factor in this gap. Because of nesting factors, the gap is not symmetric in X vs. Y , but full symmetry in k -space will reappear on averaging over spatial domains $\mathbf{Q} = (Q, 0)$, or $= (0, Q)$.

We tentatively identify the CDW gap as the d -wave pseudogap seen in the HTS materials, and identify T_{CDW} with T^* . Experimental studies show a highly inhomogeneous spatial variation of the gap [17], apparently controlled by the oxygen dopant distribution, which we interpret as a strongly impurity-pinned CDW. The regions where the gap is maximal

(75 meV - our $\chi_{\mathbf{Q}} \simeq 60$ meV), but with little sign of superconducting coherence peaks, are interpreted as the peaks in the CDW amplitude. The length scale $\simeq 40$ Å observed is similar to that predicted from Q .

We need to estimate the interaction between the two order parameters, superconducting and CDW. We calculate the CDW order parameter on the basis of the normal state, assuming that always $T_{CDW} > T_c$ ($T^* > T_c$), for which there is supporting evidence [45]. The superconducting phase - due to its small coherence length $\xi \sim 2$ nm - can coexist with the competing CDW phase [46]. We shall here describe the inhomogeneous two-order parameter coexistence phase in an approximate manner using a form of Landau-Ginzburg (LG) approach. The approach does not take into account local distortion of the superconducting order parameter by the CDW (local distortions average out, leaving perfect d -wave, over a CDW wavelength).

The LG expression for the superconducting free energy takes the form

$$F = \frac{a}{2} (\nabla \Delta)^2 + \frac{b}{2} (T - T_c^0) \Delta^2 + \frac{1}{2} \Delta^2 f(\chi^2(\mathbf{x})), \quad (23)$$

where $\chi(\mathbf{x})$ is the CDW order parameter

$$\chi(\mathbf{x}) = \chi_{\mathbf{Q}} \cos(\mathbf{Q} \cdot \mathbf{x}); \quad Q \neq 0, \quad \chi = \chi_0 / \sqrt{2}; \quad Q = 0, \quad (24)$$

$\Delta(\mathbf{x})$ is the superconducting gap, a and b and are LG parameters, T_c^0 is the transition temperature in the absence of the CDW order parameter, and f is a coupling function between the two order parameters.

In the absence of CDW order the coherence length is given by the standard formula $\xi_{LG}^0 = \sqrt{a/bT_c^0} = 0.739 \xi_{BCS}^0$; the BCS coherence length ξ_{BCS}^0 is assumed to follow BCS scaling relative to the known coherence length of the HTS. The function f is determined from solving the gap equation as a function of a spatially uniform CDW amplitude χ_0 , the input being the splitting $t_x - t_y = \chi_0$ in nearest-neighbor hopping integral. To limit order parameter distortion, a cutoff on the maximum χ is inserted, which however does not affect the conclusions.

Differentiating the free energy w.r.t. Δ we get the Schrodinger-like equation (SE) for the gap

$$-a \nabla^2 \Delta + V(\mathbf{x}) \Delta = \epsilon \Delta, \quad (25)$$

where $V(\mathbf{x}) = f(\chi^2(\mathbf{x})) - bT_c^0$, $\epsilon = -bT$. The lowest energy ϵ solution represents the highest global transition temperature $T_c = T$. The procedure is then to (1) solve for the CDW amplitude and wavevector, (2) calculate the effect on T_c of a given magnitude of uniform order parameter, and then (3) solve the SE for the transition temperature.

The results are shown in Fig. 6. We see that there is a significant reduction in T_c coming from the effect of the CDW. The isotope shift still has the same qualitative behavior, but with less variation - because χ_0 provides an additional perturbation competing with the effect of chemical potential. The STM results[17] might be more compatible with a 2D CDW than the 1D CDW assumed in this paper, and indeed tentative results for a 2D CDW show much less T_c -reduction, and enhanced isotope shift variation, but in the absence of pinning the 1D CDW is found to be more stable than the 2D one.

In the strong coupling limit, where the effect of K is larger than the effect of t , preliminary studies suggest that the FBM can produce a striped phase and a transition to an insulating state. Combined with U , a true Mott transition involving magnetism can result, leading to an RVB-like state.

We believe that this work constitutes a breakthrough in finding a natural phonon-based mechanism capable of generating a d -wave superconducting gap, a d -wave pseudogap, and giving the type of behavior of T_c , T^* , and isotope shift similar to that observed experimentally. The expected inhomogeneity of the order parameter is also observed [17]. Quantitative comparisons should bear in mind that the current picture is a highly simplified single band, single interaction parameter one. A future program of work comprises a rather long list, including first principles substantiation of the anharmonic oxygen potential and coupling to the electronic degrees of freedom, inclusion of the oxygen $2p$ -bands, calculation of spectroscopic properties such as the superconductivity-induced shift in vibrator frequency, and the phonon peaks seen in tunneling spectroscopy of the superconducting state, together with understanding the fundamental energy balance - possibly unconventional - underlying HTS. A better understanding of the CDW order and its interaction with superconductivity should be obtained from a more detailed coherent, quantum-mechanical, theoretical approach.

[1] Leggett, A.J. What do we know about high Tc ? *Nature Physics* **2**, 134-136 (2006).

[2] Bonn, D. A. Are high-temperature superconductors exotic? *Nature Physics* **2**, 159-168 (2006),

and the references therein.

- [3] Tsuei, C.C., & Kirtley, J.R. Pairing symmetry in cuprate superconductors. *Rev. Mod. Phys.* **72**, 969 (2000), and references therein.
- [4] Norman, M. R. et al., Destruction of the Fermi Surface in high- T_c superconductors. *Nature* **392**, 157-160 (1998).
- [5] Moler, K. A., et al., Magnetic field dependence of the density of states of $\text{YBa}_2\text{Cu}_3\text{O}_{6.95}$ as determined from the specific heat. *Phys. Rev. Lett.* **73**, 2744-2747 (1994).
- [6] Lee, P.A., Localized states in a d-wave superconductor. *Phys. Rev. Lett.* **71**, 1887-1890 (1993).
- [7] Taillefer, L., Lussier, B., Gagnon, R., Behnia, K. & Aubin, H. Universal heat conduction in $\text{YBa}_2\text{Cu}_3\text{O}_{6.9}$. *Phys. Rev. Lett.* **79**, 483-486 (1997).
- [8] Chiao, M. et al., Low-energy quasiparticles in cuprate superconductors: A quantitative analysis. *Phys. Rev. B.* **62**, 3554-3558 (2000).
- [9] Proust, C., et al., Heat transport in a strongly overdoped cuprate: Fermi liquid and a pure d-wave BCS superconductor. *Phys. Rev. Lett.* **89**, 147003 1-4 (2002).
- [10] Sutherland, M., et al. Thermal conductivity across the phase diagram of cuprates: low-energy quasiparticles and doping dependence of the superconducting gap. *Phys. Rev. B.* **67**, 174520 1-11 (2003).
- [11] Bel, R., et al. Test of the Wiedemann-Franz law in an optimally doped cuprate. *Phys. Rev. Lett.* **92**, 177003 1-4 (2004).
- [12] D. Achkar and M. Poirier, D. A. Bonn, Ruixing Liang, and W. N. Hardy, Temperature dependence of the in-plane penetration depth of $\text{YBa}_2\text{Cu}_3\text{O}_{6.95}$ and $\text{YBa}_2(\text{Cu}_{0.9985}\text{Zn}_{0.0015})_3\text{O}_{6.95}$ crystals from T to T^2 , *Phys. Rev. B.* **48**, 13184-113187 (1993).
- [13] X. J. Zhou, et al., Dichotomy between Nodal and Antinodal Quasiparticles in Underdoped $\text{La}_{2-x}\text{Sr}_x\text{CuO}_4$. *Phys. Rev. Lett.* **92**, 187001-187005 (2004).
- [14] Anderson, P.W., The resonating valence bond in La_2CuO_4 and superconductivity. *Science* **235**, 1196-1198 (1987); Anderson, P.W. et al., The physics behind high-temperature superconducting cuprates: the 'plain vanilla' version of RVB. *J. Phys: Condens. Mat* **16**, R755-R769 (2004).
- [15] Mourachkine A., The oxygen isotope effect on critical temperature in superconducting copper oxides. *Supercond. Sci. Techn.* **17**, 721-723 (2004).
- [16] Pringle, D.J., Williams, G.V.M., and Tallon, J.L., Effect of doping and Impurities on the

- oxygen isotope effect in high-temperature superconducting cuprates. *Phys. Rev. B.* **62**, 12527-12533 (2000).
- [17] McElroy, K., et al. Atomic-scale sources and mechanism of nanometer scale electronic disorder in $\text{Bi}_2\text{Sr}_2\text{CaCu}_2\text{O}_{8+d}$. *Science* **309**, 1048-1052 (2005), and references therein.
- [18] Opel, M., et al., Physical origin of the buckling in CuO_2 ; Electron-phonon coupling and Raman spectra. *Phys. Rev. B* **60**, 9836-9844 (1999).
- [19] Gallais, Y., Le Tacon, M., Sacuto, A., & Colson, D. Coupling between quasiparticles and a bosonic mode in the normal state of $\text{HgBa}_2\text{CuO}_{4+d}$. *cond-mat/0506711 v2* (2006).
- [20] Cuk, T., Lu, D.H., Zhou, X.J., Shen, Z.-X., Devereaux, T.P., & Nagaosa, N. A review of electron-phonon coupling seen in the high- T_c superconductors by angle-resolved photoemission studies (ARPES). *Phys. Stat. Sol. (b)* **242**, 11-29 (2005).
- [21] Cuk, T., et al. Coupling of the B_{1g} phonon to the antinodal electronic states of $\text{Bi}_2\text{Sr}_2\text{Ca}_{0.92}\text{Y}_{0.08}\text{Cu}_2\text{O}_{8+d}$. *Phys. Rev. Lett.* **95**, 117003 1-4 (2005).
- [22] Gweon, G.-H., et al., An unusual isotope effect in a high-transition-temperature superconductor. *Nature* **430**, 187-190 (2004).
- [23] Zhou, X.J., et al. Multiple bosonic mode coupling in the electron self-energy of $(\text{La}_{2-x}\text{Sr}_x)\text{CuO}_4$. *Phys. Rev. Lett.* **95**, 117001 1-4 (2005).
- [24] Pintschovius, L., et al. Oxygen phonon branches in $\text{YBa}_2\text{Cu}_3\text{O}_7$. *Phys. Rev. B* **69**, 214506 1-11 (2004).
- [25] Saini, N. L., et al., Evidence for local lattice fluctuations as a response function of the charge stripe order in the $\text{La}_{1.48}\text{Nd}_{0.4}\text{Sr}_{0.12}\text{CuO}_4$ system. *Phys. Rev. B* **64**, 132510 1-4 (2001).
- [26] Lee, J., et al, Vizualizing the influence of nanoscale electron-lattice interactions on high- T_c superconductivity in $\text{Bi}_2\text{Sr}_2\text{CaCu}_2\text{O}_{8+\delta}$ (to be published).
- [27] Khasanov, R., Shengelaya, A., Morenzoni, E., Conder, K., Savic, M.I., & Keller, H. The oxygen isotope on the in-plane penetration depth in cuprate superconductors. *L. Phys.: Condens. Matter* **16**, S4439-S4455 (2004).
- [28] Bussmann-Holder, A., & Bishop, A.R., Anharmonicity-induced multiphonon processes in high-temperature superconductors. *Phys. Rev.* **44**, 2853-2856 (1991).
- [29] Bussmann-Holder, A., & Keller, H. Polaron formation as origin of unconventional isotope effects in cuprate superconductors. *Eur. Phys. J. B* **44**, 487-490 (2005). and the references therein.

- [30] Muller, K.A., From Single to Bi-polarons with Jahn-Teller character and metallic cluster-stripes in hole-doped cuprates. To be published in "Treatise on High Temperature Superconductivity", edited by J.R. Schrieffer.
- [31] Crespi, Vincent H., & Cohen, Marvin L. Anharmonic phonons and high-temperature superconductivity. *Phys. Rev.* **48**, 398-406 (1993).
- [32] Kubic, M.L., Interplay of electron-phonon interaction and strong correlations: the possible way to high-temperature superconductivity. *Phys. Repts.* **338**, 1-264 (2000).
- [33] Cappelluti, E. & Pietronero, L., Nonadiabatic superconductivity: The role of van Hove singularities. *Phys. Rev. B.* **53**, 932-944 (1996).
- [34] Sakai, T., Poilblanc, D., & Scalapino, D., Hole pairing and phonon dynamics in generalized two-dimensional $t - J$ Holstein Models. *Phys. Rev. B.* **55**, 8445-8451 (1997).
- [35] Seidel, A., Lin, H.-H., & Lee, D.-H., Phonons in Hubbard ladders studied within the framework of the one-loop renormalization group. *Phys. Rev. B.* **71**, 220501-220505 (2005).
- [36] Schuttler, H.-B., & Pao, C.-H., Isotope effect in d-wave superconductors. *Phys. Rev. Lett.* **75**, 4504-4507 (1995).
- [37] Lines, M.E., and Glass, A.M., Principles and Applications of Ferroelectrics and related Materials, Clarendon Press, Oxford UK (1979), and references therein.
- [38] Büchner, B., Breuer, M., Freimuth, A. & Kampf, A. P., Critical buckling for the disappearance of superconductivity in rare-earth-doped $\text{La}_{2-x}\text{Sr}_x\text{CuO}_4$. *Phys. Rev. Lett.* **73**, 1841-1844 (1994); Chmaissem, O. et al., Scaling of transition temperature and CuO_2 plane buckling in a high-temperature superconductor. *Nature* **397**, 45-48 (1999).
- [39] Read, N., and Newns, D.M., On the Solution to the Coqblin-Schrieffer Hamiltonian by the Large-N expansion Technique. *J. Phys. C.* **16**, 3273-3295 (1983); Bickers, N.E., Review of techniques in the large-N expansion for dilute magnetic alloys. *Rev. Mod. Phys.* **59**, 845-939 (1987), and references therein.
- [40] Coleman, S., Aspects of Symmetry. Cambridge, New York, (1985).
- [41] Lavagna, M., Millis, A.J. & Lee, P.A., d -wave superconductivity in the large-degeneracy limit of the Anderson lattice. *Phys. Rev. Lett.* **58**, 266-269 (1987); Kotliar, G. & Liu, J., Superconducting Instabilities in the Large-U Limit of a Generalized Hubbard Model. *Phys. Rev. Lett.* **61**, 1784-1787 (1988); Sudbø, A., and Houghton, A., Charge fluctuations, Spin fluctuations and superconductivity in a CuO_2 sheet. *Phys. Rev. B.* **42**, 4105-4116 (1990).

- [42] Serene, J. W., & Hess, D. W., Quasiparticle properties of the two-dimensional Hubbard model in a propagator-renormalized fluctuation-exchange approximation. *Phys. Rev. B.* **44**, 3391-3394 (1991).
- [43] Presland, M. R., Tallon, J. L., Buckley, R. G., Liu R. S. , & Flower, N. E., General trends in oxygen stoichiometry effects on Tc in Bi and Tl superconductors. *Physica (Amsterdam)* **176C**, 95-105 (1991).
- [44] Grüner, G., The Dynamics of Charge Density Waves. *Rev. Mod. Phys.* **60**, 1129-1138 (1988), and references therein.
- [45] Shibauchi, T., Krusin-Elbaum, L., Li, Ming, Maley, M. P., & Kes P. H., Closing the Pseudogap by Zeeman Splitting in $\text{Bi}_2\text{Sr}_2\text{CaCu}_2\text{O}_{8+y}$ at High Magnetic Fields. *Phys. Rev. Lett.* **86**, 5763-5767 (2001); Timusk, T. & Statt, B., The pseudogap in high-temperature superconductors. *Rept. Progr. Phys.* **62**, 61-82 (1999).
- [46] Machide, K., Koyama, T., & Matsubara, T., Theory of charge-density-wave superconductors. *Phys. Rev. B* **23**, 99-105 (1981).

Acknowledgments

Both authors contributed equally to this work. Correspondence should be addressed to D.M.N at dennism@us.ibm.com